THE JOURNAL OF PHYSICAL CHEMISTRY B

ARTICLE

pubs.acs.org/JPCB

Quantitative Analysis of Aqueous Nanofilm Rupture by Molecular Dynamic Simulation

Tiefeng Peng,[†] Anh V. Nguyen,[*,†] Hong Peng,[†] and Liem X. Dang[*,‡]

[†]School of Chemical Engineering, The University of Queensland, Brisbane, QLD 4072, Australia

[‡]Pacific Northwest National Laboratory, Richland, Washington 99352, United States

ABSTRACT: In this study, we used molecular dynamics (MD) simulations of the rupture process for a water film to define and determine the critical rupture time (CRT). This new approach could be an important method for authentically defining and determining the rupture point of a water film and associated phenomena. We were able to predict generically the CRT and the critical thickness of the water film. Then, we studied the effect of ions on the film rupture process. Our results showed that the addition of sodium chloride did not significantly affect the stability of the water film. Results from MD simulations, when compared with results from experimental measurements, can provide insight into the film rupture process.

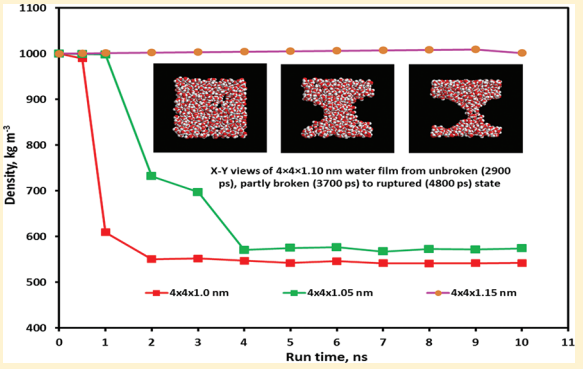

1. INTRODUCTION

Many experiments have been undertaken to investigate the film rupture process.[1−6] In the first stage of liquid film drainage, when a relatively thick liquid phase exists between air bubbles, gravity plays an important role. When the thickness decreases to ∼100 nm, the gravity effect becomes negligible, and interfacial interactions, including electrostatic, dispersion, and hydration forces, begin to be major factors in film drainage and rupture.

The experiment is the comprehensive result of many environmental effects:[7−10] random motion of microscopic particles, collisions of surrounding gas molecules, atmospheric humidity, and so on. Using microinterferometry, Karakashev et al.[7] reported the effects of ions on film rupture, and the lifetime of aqueous foam films formed from sodium chloride (NaCl), lithium chloride (LiCl), sodium acetate (NaAc), and sodium chlorate ($NaClO_3$). They found that relatively long-lasting and nondraining films prepared from salt solutions above 0.1 M could be observed. The film lifetime was significantly longer by one to two orders of magnitude (i.e., from 10 to 100 s). Also, both the film lifetime and the (average) thickness of the nondraining films increased with increasing salt concentration. This effect has not been observed with foam films stabilized by surfactants. The film lifetime and thickness also increased with increasing film radius. From all of these experiments, the thickness order was usually ∼100 nm, which is a very different value from the thicknesses, obtained using computer simulations. Experiments using microinterferometry showed that foam films of ultrapure deionized (DI) water can last up to 10 s, and the contact time between two gas bubble surfaces at close proximity significantly influences the film drainage, rupture, and lifetime.[8−10] Yang and coworkers have performed simulations to investigate the water/surfactant film rupture to predict the stability of water/surfactant film. In general, the simulation results are in reasonable agreement with the corresponding experimental results.[11,12] Faraudo and Goddard have also reported computer simulation studies on the Newton black films.[13,14]

Recent experiments have suggested that nanobubbles can stably form at a hydrophobic surface and in an aqueous solution[15,16] and can be used to explain the liquid film rupture through a number of stages.[17,18] For example, during film drainage between a large air bubble and a hydrophobic surface, the macroscopic bubble first approaches the apex of the largest surface nanobubbles. A nanometer-sized aqueous foam film is effectively formed between the macroscopic bubble and the nanobubble, where the van der Waals attraction is strong. The attractive van der Waals force can destabilize the film locally as traditionally proposed.[19] The local film destabilization can be increased further by the increase in the local capillary pressure because of the concave surface of the nanobubble, resulting in the disappearance of the entire macroscopic film. Understanding the rupture of the nanofilms evidently is critical to the nanobubble theory on the rupture of macroscopic films. Unfortunately, the nanofilms could not be directly visualized and examined because of the limited optical resolution that is available. Therefore, MD simulation studies of nanofilm rupture would be extremely useful.

Computer simulations and experimental measurements have been used widely in attempts to understand chemical phenomena in bulk liquids and at liquid−air, liquid−liquid, and liquid−solid interfaces.[20−28] Applying these efforts to the discovery of fluid properties can be a very promising research method.

Received: September 15, 2011
Revised: November 14, 2011
Published: December 15, 2011

Knowledge of liquid−film systems is important for understanding industrial processes such as phase separation, flotation separation of particle using gas bubbles, water desalination, and so on. Aqueous film systems could be classified mainly as water films containing ions or liquid films containing surfactants. From the perspective of MD simulations and given the experimental complications associated with the studies of thin films, it makes sense to combine experimental approaches with computational studies to discover new insights that can be used to interpret the fundamental aspects of the phenomena. In this Article, we present a new model—critical rupture time (CRT)—and propose new criteria for defining and determining the critical thickness and CRT of the film, which, in turn, could be used to distinguish accurately the rupture point based on user-selected parameters. We used the Gibbs dividing area, two stable states, and the correlation between CRT and critical thickness of the aqueous film to predict the critical thickness and CRT. Then, using a pure water film as a reference, we determined the effect of ions on the film rupture process. The results of our simulations also were compared with results obtained from experiments.

This Article is organized as follows. The molecular models and simulation details are described in Section 2. The water-film rupture process associated with time, the water-film size, and the effects of ions are presented and discussed in Section 3. The conclusions and future research directions are presented in Section 4.

2. COMPUTATIONAL DETAILS

2.1. Molecular Models and MD Parameters. MD simulations were performed using the *GROMACS* software package 4.5.3.[29−32] In addition, the ion parameters used were specified within the OPLS-AA force field, which were in the data files corresponding to the *GROMACS* distribution. The MD model for water was a simple extended point-charge model,[33] as it could reproduce thermodynamic properties at a relatively low computational cost. In future work, we will employ potential models that take many-body effects into account.[34] Long-range electrostatic interactions were treated by the particle mesh Ewald.[35] The Lennard-Jones and Coulombic interactions both had a real space cutoff fixed at 14 Å. All simulations were undertaken at a time step of 1 fs. Temperature coupling used the v-rescale method at a constant temperature of 300 K with a time coupling of 0.1 ps. The velocity-rescaling thermostat is essentially a Berendsen thermostat, which can produce a correct canonical ensemble and still have the advantages of the Berendsen thermostat.[36]

2.2. Simulation Procedure. We first created the film using *GROMACS* by defining the lateral scale ($L_x = L_y$) and the thickness of film in three dimensions. We then put the film at the center of a vacuum box ($L_x = L_y = L_z/3$) to simulate the liquid−vapor interface. A slab geometry was employed as follows: the size of the box was set to $L_x = L_y$, $L_z = 3L_x$; the lateral sizes ($L_x = L_y$) of film had the same value as the lateral dimensions of the box, and the Z dimension of the film was centered in the box with the two surfaces perpendicular to the Z axis. The overall packing of water films for the initial configuration was close to the experimental density of water (1000 kg m^{-3}).

Some water molecules could escape from the water layer during the simulation. The water molecules and ions were randomly packed into their corresponding boxes. The run times were 11 ns for most water films, 11 ns for films with ions in critical thickness range (Gibbs dividing range in Section 3.3), and 3 ns for films with ions not in Gibbs dividing range. The first 500 ps was used as an equilibration period in the NVT ensemble. For water films, 5 lateral sizes (3 × 3, 4 × 4, 6 × 6, 8 × 8, 10 × 10 nm) and 10 simulation durations (1 to 10 ns) were chosen to study the simulation results. The film L_z value ranged from 0.7 to 1.5 nm. For films with Na^+ and Cl^- ions, the 3 × 3 nm film contained 8 ions, the 4 × 4 nm film contained 15 ions, and the 6 × 6 nm film contained 30 ions. The critical thickness could be determined from the density profile results, and CRT can be obtained by studying the certain size of a film, which ran for 11 ns, applying density and combining with trajectory snapshots to judge the rupture.

Table 1. (Maximum) Density (kg m^{-3}) of Water Films Versus Run Time[a]

run time (ns)	film dimensions ($L_x \times L_y \times L_z$) (nm^3)	
	4 × 4 × 1.05	4 × 4 × 1.10
0.5−1	998.77	1006.60
1	997.85	1001.04
2	731.91	1000.90
3	697.14	905.50
4	570.59	733.01
5	575.13	745.72
6	576.58	748.03
7	567.37	741.03
8	572.44	750.67
9	571.33	746.73
10	574.13	749.70

[a] 0.5−1 means the data were collected from 500 to 1000 ps duration, and 1 means that data were collected from 1000 to 2000 ps, and so on.

3. RESULTS AND DISCUSSIONS

3.1. From Thin Film Rupture Process to Define CRT. *3.1.1. Introduction for the Criteria of Critical Density Percentage.* To introduce CRT, 4 × 4 × 1.05 and 4 × 4 × 1.10 nm water films were selected as examples to illustrate our methodology. When defining the CRT, the dimensions of the film should be fixed ($L_x = L_y$, L_z, all fixed), and the water density inside the film versus run time of MD simulation was monitored and assessed. Typical results for the maximum density along the Z dimension as collected at different run times are shown in Table 1. All density profiles were collected along the Z axis with the box size L_z partitioned into 200 parts to calculate density; here L_z is a box size of the Z dimension, not the film thickness. Figure 1 shows the density profiles versus the number of box partitions along the Z dimension for the 4 × 4 × 1.05 nm water film. It is evident from Figure 1 that if the number of box partitions is not greater than 50 then collected density cannot represent the real density profile correctly. Likewise, if the L_z was too large, then 50 partitions would be unsuitable. When the number of box partitions is ≥100 (e.g., 200 or 400), the simulation provides a consistent density trend. Therefore, 200 box partitions were used for our simulation. As shown from the data in Table 1, the density decreases as the run time increases, and the density does not change significantly at long run times. For example, the density of the 4 × 4 × 1.05 nm film fluctuates around ∼570 kg m^{-3} after 4 ns. Figure 2 shows snapshots of a 4 × 4 × 1.10 nm water film from the unbroken state to the ruptured film state. Holes are

stochastically formed within a film; however, they can further expand, which will lead to film rupture or collapse, making the film stable. The criterion then should be chosen to define CRT. In general, the film rupture starts with the formation of a hole. Therefore, direct evidence of film rupture could be obtained by identifying a hole within a film from the snapshots and the trajectory of the system. However, more accurate evidence could be achieved from the density profile.

For the 4 × 4 × 1.10 nm water film, an average density of 905.50 kg m^{-3} was obtained at 3 to 4 ns. The snapshot taken at 3700 ps (Figure 2) shows that the water film was not intact (as a reference, the time point at 2900 ps could be regarded as intact) even though the density was 905.50 kg m^{-3}. Holes were present in the film; no droplets had formed at 3 to 4 ns. Therefore, even though the density was >900 kg m^{-3}, the water film can still have holes. If a film has holes, then it is to some degree broken but not enough for droplets to form. Therefore, from the density profile of the 4 × 4 × 1.10 nm water film and the snapshots in Figure 2, we concluded that if the density is <900 kg m^{-3}, then the film is not intact.

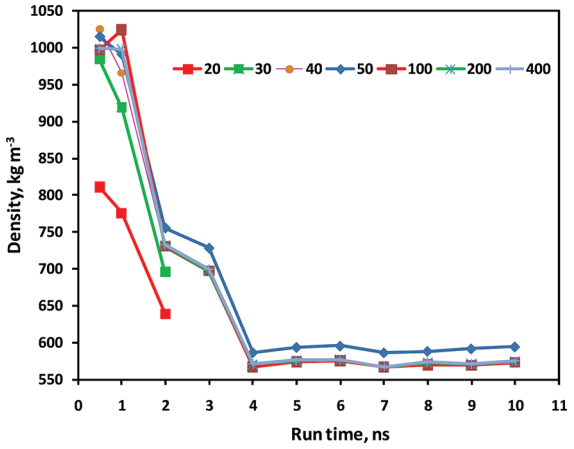

Figure 1. Effect of the number of box partitions along the *Z* dimension on the transient profile of (maximum) density for 4 × 4 × 1.05 nm water film. The legend shows the number of partitions of the simulation box.

To extend the application of this methodology to other liquid films (e.g., H-bonding molecular films such as ethanol and polyalcohol or non-H-bonding molecular films such as aldehydes and ketones), we can set the intact film as having 100% liquid density, and the nonintact film as a lower percentage (e.g., 90, 80, 60%, etc.) according to the responding condition, which will be a user-selected parameter to define its critical value according to a specific purpose. The choice of the percentage (a standard of critical value [e.g., 90, 80, 60%, etc.]) for this parameter depends on the final goal of the research, which can be input for the next modeling step (e.g., the bubble coalescence or bubble-particle attachment, the aging process of aqueous foams [several stages can be distinguished in the foam lifetime], etc.).

With different research goals, different critical density percentages can be used to define the CRT. To study the phenomena associated with the film in the early rupture stage, one can select 90%; however, if area of interest is in the middle phase, then 75% might be chosen. Finally, if the goal is to investigate the influence or result of the droplets, then 60% (i.e., a film that has severely broken into droplets) could be the choice.

In our research, we were concerned with the beginning of the rupture, so 90% was selected to define the CRT. We chose 900 kg m^{-3} as the standard critical density value for defining the CRT even though the choice was somewhat arbitrary. We also could have chosen 901 or 899 kg m^{-3} as the critical density for determining the CRT. However, if the average density at a certain time duration (e.g., between the *n* and *n* + 1 steps of run times [ns]) was >900 but <950 kg m^{-3}, then the film is considered to be broken to some degree. Early in this 1 ns duration simulation, the film may be intact; however, later in the simulation, holes formed in the water film. Therefore, if the average density was <850 kg m^{-3}, then the film would be considered to be broken at the end of the 1 ns simulation.

3.1.2. Illustration for the Determination of CRT. The data presented in Table 1 show that after the film ruptured the density fluctuated at a level. Using a 4 × 4 × 1.10 nm water film as a

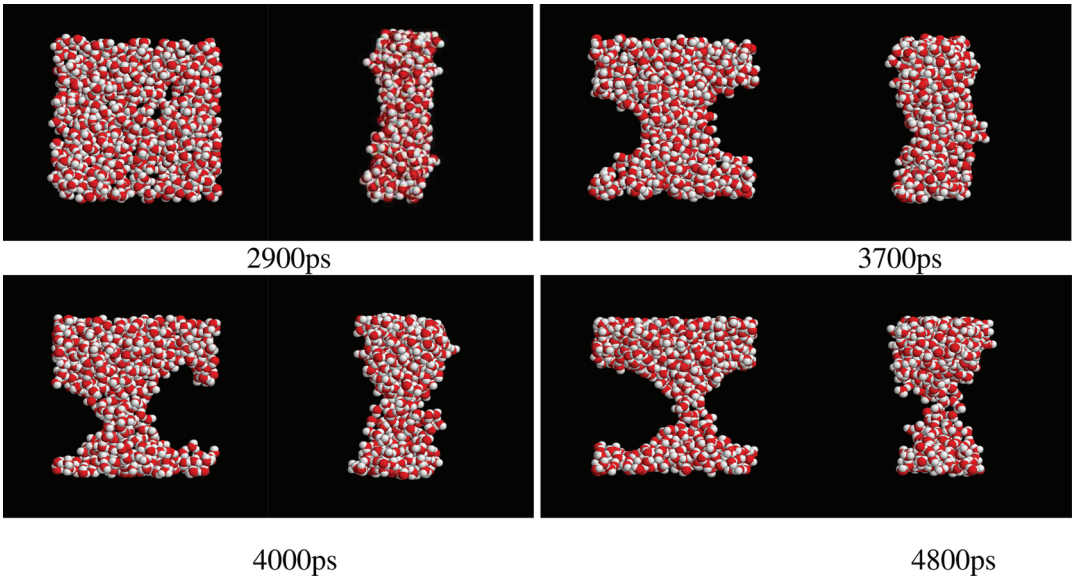

Figure 2. *X*−*Y* (left) and *X*−*Z* (right) views of 4 × 4 × 1.10 nm water film from unbroken (2900 ps), partially broken (3700, 4000 ps), to ruptured (4800 ps) state. Many holes within the film were formed at the ruptured states.

dx.doi.org/10.1021/jp208896y |*J. Phys. Chem. B* 2012, 116, 1035–1042

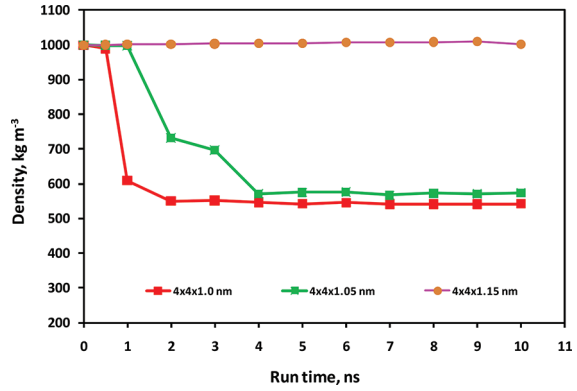

Figure 3. Typical density plots to introduce CRT: Density of lateral size 4 × 4 nm films versus run time. The CRT for the 4 × 4 × 1.100, 4 × 4 × 1.105, and 4 × 4 × 1.15 nm films are approximately 1 ns, 2 ns, and infinity, respectively.

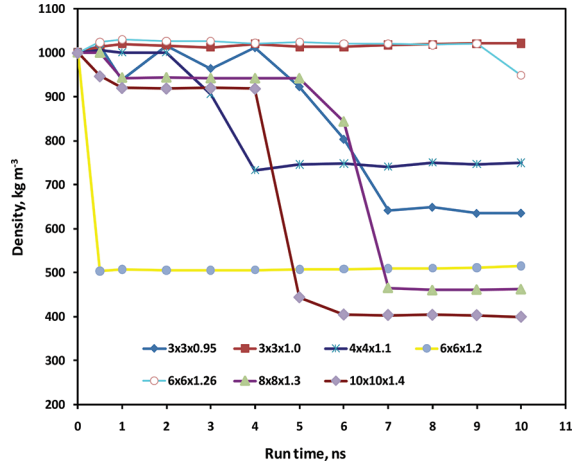

Figure 4. Computed density profiles of some films versus simulation run time.

typical example, the CRT should satisfy the following two requirements

(1) At a 4 ns duration, the density should be <90% (900 kg m^{-3}).
(2) At a 4 ns duration, the density should be <90% (900 kg m^{-3}) for the first time.

In Figure 3, we show a typical plot to introduce CRT using lateral size 4 × 4 nm films as an example.

To achieve a reasonable and consistent research approach, we considered 1 ns to be the CRT for a 4 × 4 × 1.10 nm water film. (See Figure 4.) Following this principle, the CRT for a 4 × 4 × 1.05 nm water film would be 2 ns. Figure 4 shows the profiles of density versus simulation run time. When the ratio $L_x = L_y/L_z$ was different, the final ruptured shapes of films (a series of films with the same $L_x = L_y$ [e.g., as shown in Figure 3]) could be different. For a given water film with a fixed size (e.g., see Figure 2), the ruptured shape could be estimated by changing the run time. For different water films, the ruptured shapes also differed. For example, it is not easy for a 4 × 4 × 1.10 nm water film to form droplets even with a long run time. For some films (e.g., a 4 × 4 × 1.30 nm water film), a certain shape cannot be achieved because the film will not rupture within a limited run time. For a water film with an L_z close to or a slightly larger than its critical thickness (please see the Gibbs dividing range in Section 3.3), it is not easy for the liquid to form droplets. If the value of the L_z is less than its critical thickness, then the water film could break into droplets and then form an aggregate (which also could be regarded as a droplet state).

Table 2. Density of Water Films with $L_x = L_y = 4$ nm, $L_z = 0.7$ to 1.3 nm, and Run Time = 2 ns

L_z, nm	0.7	0.8	0.9	1.0	1.1	1.2	1.3
density, kg m^{-3}	464.68	493.10	533.64	613.30	1001.04	999.08	1000.49

From Figure 4, when L_z was close to the critical thickness (within the Gibbs dividing range; see Section 3.3) of the film, the density change was sensitive at the rupture point. For 3 × 3 × 0.95 and 4 × 4 × 1.10 nm water films, the final densities were between 600 and 800 kg m^{-3} within 10 ns, whereas for 4 × 4 × 1.05 (in Figure 3) and 10 × 10 × 1.40 nm water films, the final densities were between 400 and 600 kg m^{-3}. The reason for this behavior was previously explained; that is, when the $L_x = L_y/L_z$ value was different, the ruptured shapes could be different, so the density profile of the final stage was correspondingly different. From the data shown in the Figures and the Table cited thus far, we noted that after the film ruptured and even at prolonged the run times the density does not change much. Rather, it just fluctuates around an ultimately achieved value.

3.1.3. Classification of Films Based on Their Corresponding CRTs. From Table 1 and Figure 4, it can be seen that for a 4 × 4 × 1.10 nm water film the rupture time is ~4 ns. This kind of film could be stable for a short time. The 4 × 4 × 1.0 and 6 × 6 × 1.2 nm films actually could exist for a very short time, or they could rupture at the beginning. The 4 × 4 × 1.15 and 3 × 3 × 1.0 nm films as shown in Figures 3 and 4, respectively, could have larger CRT values. When the CRT of a film was infinity (meaning the film will not rupture within a limited time), the film could be considered to be a "stable film." When the film could have a very large CRT, it was considered to be a "critical film," in which the *Z*-dimensional thickness would be between the thickness of a "thin film" and a "stable film." A "thin film" has a medium CRT lying between the CRTs of a "ruptured film" and a "critical film." The thinnest film is the type that could rupture in a very short time, and it appears that this kind of film could rupture at the beginning of film formation. We established the following classifications to distinguish the four types of films: (1) ruptured film, (2) thin film, (3) critical film, and (4) stable film.

Some films that are close to their critical thickness (at the Gibbs dividing range discussed in Section 3.3) had medium CRT values. If they had large CRT values, then their density at the first 11 ns would be ~1000 kg m^{-3}. From thermodynamics and the MD study, two stable states (see Section 3.3) are achieved for liquid films after long simulation run times. These stable states are observed in the results obtained from both experiments and MD simulations. One state is 100% (CRT = infinity), and the other is the ruptured film state. If a certain film has a CRT = A ($0 < A < \infty$), after running for a long time, then the film could finally change into droplets.

3.2. New Criterion for Defining and Determining the Critical Thickness. To determine the critical thickness, we performed MD simulations for different thicknesses and film lateral dimensions at a given constant simulation run time. Table 2 shows the results obtained with a selected run time of

2 ns. When calculating density, one could selectively collect certain periods from the whole run time. For the data presented in Table 2, durations ranging from 1000 to 2000 ps were selected to collect data needed to calculate density. Therefore, for the results discussed below in Sections 3.3 and 3.4, data from the last 1 ns of the simulation were applied to calculate density.

In general, if the density was lower than 900 kg m^{-3}, then the film was not intact. From Table 2, when $L_z \leq 1.0$, the film was broken. Therefore, one should decide which value of thickness is the critical thickness. One method we used was to set a critical density standard to define critical thickness; for example, 800 kg m^{-3} could be selected as the critical rupture density standard. This means that if the density >800 kg m^{-3}, then the film could be considered to be unbroken. Therefore, for the film ($L_x = L_y = 4$) in Table 2, the critical thickness could be between 1.0 and 1.1 nm, so one could select 1.05 nm. This method is based on the severity of the break associated with the density profile. This means that if one selects 600 kg m^{-3} as the critical rupture density, then the critical thickness could be 0.95 nm.

Similarly, following the methodology described for CRT in Section 3.1, 90% was applied here as the user-selected density to identify the critical rupture point. Another method for defining the critical thickness would be to apply accurate dynamic phenomenon. From Table 2, the density did not change dramatically when $L_z \leq 1.0$; however, when $1.0 < L_z < 1.1$, the density changed dramatically (within the Gibbs dividing range discussed in Section 3.3). Therefore, if one arbitrarily chooses 600 kg m^{-3} as the critical rupture density standard, then the true dynamic phenomenon will not be reflected. Therefore, the value chosen for the critical density should always be within the Gibbs dividing range.

Using water film $L_x = L_y = 4$ nm as an example, the critical thickness can be easily within between 1.0 nm and 1.1 nm (Figure 5). When $L_x = L_y = 4$ nm and $L_z = 1.05$ nm and if the final density was >900 kg m^{-3}, then the critical thickness could be between 1.0 and 1.05 nm; if the final density was <900 kg m^{-3}, then the critical thickness could be between 1.05 and 1.10 nm. In fact, the critical thickness could be obtained more precisely by continuing to divide as shown above. The density changed considerably when the value of L_z was close to its critical thickness.

Comparing the definitions of CRT and critical thickness reveals that when the rupture occurs (in Section 3.3, CRT = A), then after that CRT time point or if the value of L_z changes slightly, the film state changes dramatically from unbroken state to broken. For the definition of CRT (fixed film size) and with a prolonged time, the density exhibits a decreasing trend and fluctuates at a constant value during the final stages of the simulation. At a critical film thickness (fixed time), the density decreases significantly at an L_z thickness (within the Gibbs dividing range) close to the critical thickness. The two terms indicate that the system changes significantly at the critical points.

3.3. Gibbs Dividing Area, Two Stable States, Correlation between the CRT and the Critical Thickness of the Aqueous Film. To propose the Gibbs dividing area (i.e., the Gibbs dividing range) and the two stable film states, we show a typical plot of density versus thickness in Figure 6. The term D is the Gibbs dividing range, $D = L_2 - L_1$, where L_2 and L_1 describe the film thicknesses of a density value of 100 and 60%, respectively. The Gibbs dividing range is the range $[L_1, L_2]$. When a film thickness L is within $[L_1, L_2]$, the film is not in its stable state. The CRT and critical thickness are sensitive to the change in the run time and film thickness only within the Gibbs dividing range. This Gibbs dividing range serves as a reference for interpreting results in Sections 3.1 and 3.2. If a film (the film size is fixed) has a plot similar to the plot in Figure 6, then it has a CRT = A (where $0 < A < \infty$). If one film does not have a plot similar to Figure 6 (with a finite run time between A and ∞), then this type of film has either CRT = infinity (at the right side of L_2) or a CRT = 0 (at the left side of L_1). When time is fixed, there are two stable film states. When the film thickness, L, is larger than "L_2," the density is 100%; when L is smaller than "L_1," the film forms droplets but is also in a stable state. From Figure 7, the plot will shift to the right side slightly when the run time increases. For a given film, the Gibbs dividing range $[L_1, L_2]$ will change slightly, whereas its

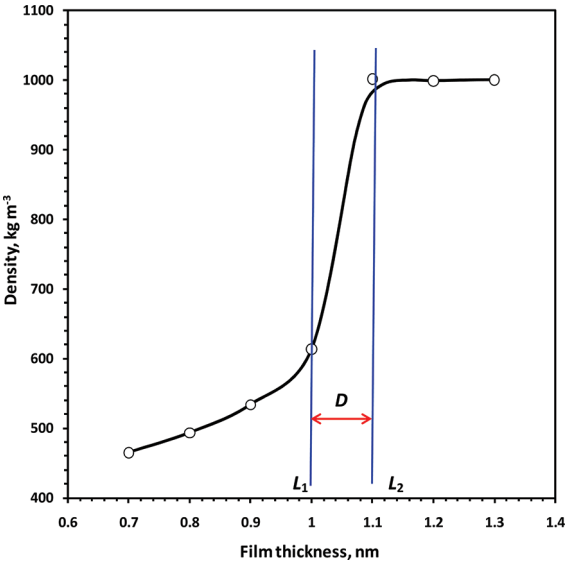

Figure 6. Illustrational plot of density versus film thickness to define Gibbs dividing surface range.

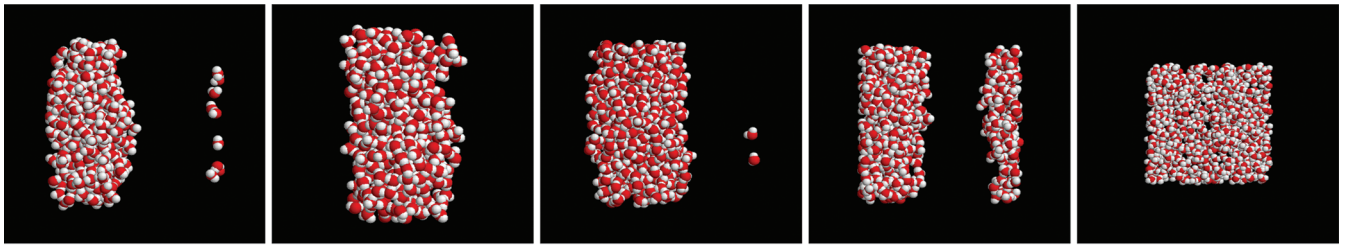

Figure 5. $X-Y$ View snapshots of $L_x = L_y = 4$ nm after 2 ns, for film thickness $L = 0.7$ to 1.3 nm.

dx.doi.org/10.1021/jp208896y |J. Phys. Chem. B 2012, 116, 1035–1042

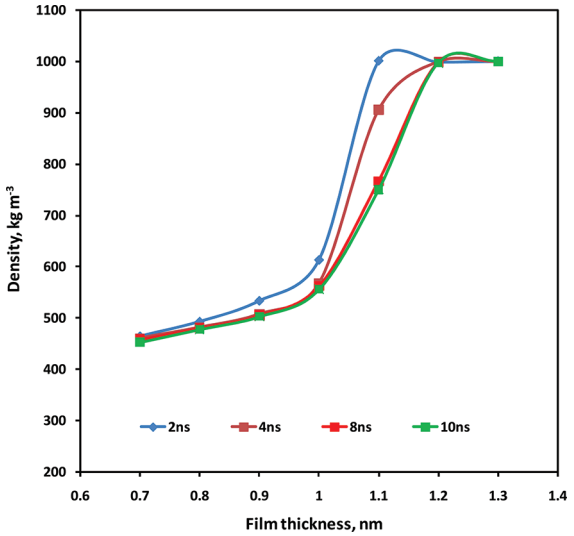

Figure 7. Computed density versus thickness for film 4 × 4 nm for different run times.

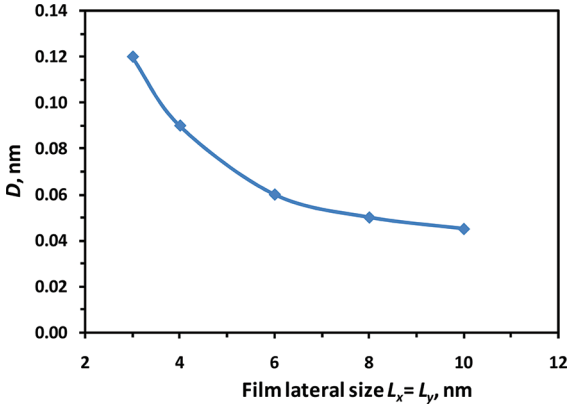

Figure 8. Computed Gibbs dividing range versus film lateral dimension ($L_x = L_y$ = 3, 4, 6, 8, 10 nm).

D value usually will not change significantly. On the basis of the knowledge that D changed very slightly, we plotted D versus the film lateral scale $L_x = L_y$ in Figure 8. The results showed that when the $L_x = L_y$ became larger, its corresponding D value would gradually decrease. In general, half of the Gibbs area is at 75 to 80% densities, which is similar to the usual interface definition used in the literature.

3.4. Prediction of CRT and Critical Thickness. *3.4.1. Prediction of CRT.* CRTs and critical thicknesses of water films are provided in Tables 3 and 4, respectively. From Table 3, when the value of the lateral size ($L_x = L_y$) becomes larger, its associated CRT becomes more sensitive. When the lateral size is small (e.g., 3 × 3 nm), its thickness L must have a larger range of D to have a medium CRT. However, when the $L_x = L_y$ is large, the same range of L could result in the CRT changing from zero (i.e., a ruptured film) to a very large CRT. This is similar to the trend of D versus the lateral dimension. From Table 3, it is not possible to predict CRT. Table 4 lists critical thicknesses of some water films versus time.

In general, when the lateral size is fixed, the critical thickness does not increase considerably with increasing run time. Figure 9 shows a plot of critical thicknesses versus run time for 4 × 4 nm

Table 3. CRT of Some Water Films

film dimensions ($L_x \times L_y \times L_z$) (nm^3)	CRT (ns)
3 × 3 × 0.80	ruptured film
3 × 3 × 0.90	3
3 × 3 × 0.95	5
3 × 3 × 1.00	>10
4 × 4 × 1.00	ruptured film
4 × 4 × 1.05	2
4 × 4 × 1.10	4
4 × 4 × 1.15	>10
6 × 6 × 1.20	ruptured film
6 × 6 × 1.26	10
8 × 8 × 1.30	6
8 × 8 × 1.37	>10
10 × 10 × 1.40	5
10 × 10 × 1.50	>10

Table 4. Critical Thickness (nm) of Water Films Versus Run Time

time (ns)	lateral dimensions ($L_x \times L_y$) (nm^2)				
	3 × 3	4 × 4	6 × 6	8 × 8	10 × 10
1	0.85	1.04	1.20	1.27	1.32
2	0.87	1.05	1.20	1.27	1.33
3	0.90	1.07	1.22	1.28	1.35
4	0.92	1.09	1.23	1.29	1.37
5	0.94	1.10	1.24	1.30	1.40
6	0.95	1.11	1.26	1.31	1.41
7	0.96	1.11	1.26	1.33	1.42
8	0.96	1.12	1.26	1.36	1.44
9	0.97	1.13	1.27	1.37	1.45
10	0.99	1.14	1.27	1.37	1.45

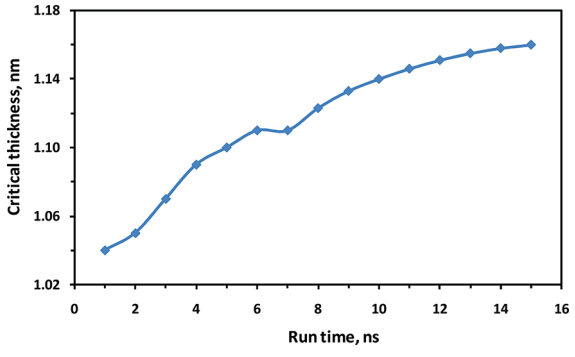

Figure 9. Computed critical thicknesses versus run time for lateral size 4 × 4 nm water films.

films, which serves as a typical example for predicting the CRT. In Figure 9, the plot levels off over a prolonged run time. If the value of the L thickness is small (i.e., not in a stable state), then its H-bonding network is not strong enough to keep the water molecules stable, so the film would tend to rupture over time. When the film is stable (CRT = 0, droplet state; CRT = infinity, always intact film), the cohesive force—H-bonding

dx.doi.org/10.1021/jp208896y |J. Phys. Chem. B 2012, 116, 1035–1042

(H-bonding due to Coulombic-static force) can keep the water molecules in their equilibrium position, but the molecules can still vibrate and fluctuate slightly. It is obvious that with increasing temperature the molecules vibrate more rapidly, and the film becomes more likely to rupture and form droplets. According to thermodynamic theory and MD simulation, the two final stable states result from the van der Waals force and the Coulombic-static force. By fitting this plot, an equation is obtained as follows: $L = -0.21874^{-0.0662CRT} + 1.25$, where the film thickness is in nanometers and the CRT is in nanoseconds.

3.4.2. Prediction of Critical Thickness. Critical thicknesses of the water films are provided in Table 4. The plot of critical thickness versus the reciprocal of corresponding run time, $1/T$, is shown in Figure 10 using data from Table 4. From Figure 10, it can be seen that prolonging the run time allows the critical thickness to converge. A final critical thickness can be determined through data fitting when the run time approaches infinity. With a prolonged run time, the trend would level off. (See the 4×4 and 8×8 nm films in Figure 10.) Here the $1/T$ value is too narrow to see the trend.

3.5. Effect of Ions on Film Rupture. The simulation run time was 3 ns for the films with ions. The thinner (e.g., $3 \times 3 \times 0.8$ nm) film was ruptured, and the thicker (e.g., $3 \times 3 \times 1.0$, $4 \times 4 \times 1.15$, $6 \times 6 \times 1.3$ nm) water film was unbroken. These films were used as references to study the effect of ions on film rupture. Here 8 ions (eight Na^+ and eight Cl^- ions) were added to the 3×3 nm films, 15 ions to the 4×4 nm films, and 30 ions to 6×6 nm films. Table 5 shows the film states after running for 3 ns. From the results for $3 \times 3 \times 1.0$, $4 \times 4 \times 1.15$, and $6 \times 6 \times 1.3$ nm films, it can be concluded that Na^+ and Cl^- ions do not break the films. This finding means that the presence of NaCl does not have an adverse effect on the nanofilm stability. On the basis of experimental results, the NaCl ion effect on film stability is weak because Na^+ and Cl^- ions are small; therefore, they are strongly hydrated and form strong iron pairing within the film. However, compared with large ions and molecules such as surfactants (e.g., sodium dodecyl sulfate), the NaCl salt ions are not strong in stabilizing water films. The salt can only slightly influence the transient stability of the films, which can be important in the flotation separation of hydrophobic particles.

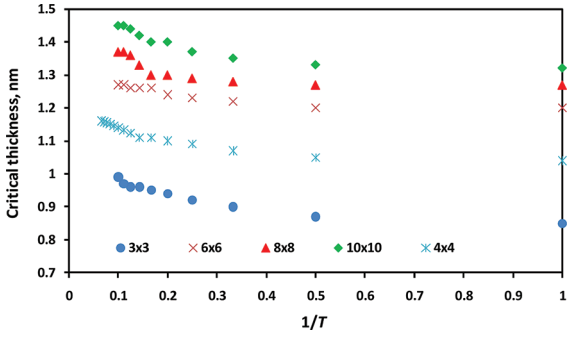

Figure 10. Computed critical film thickness versus reciprocal of its run time (ns), $1/T$.

To investigate the effect of ions on a film thickness L close to the critical thickness (within the Gibbs dividing range), we applied a $5 \times 5 \times 1.14$ nm water film running for 11 ns as reference. This water film ruptured at 4300 ps. By adding 22 Na^+ and Cl^- ions, the $5 \times 5 \times 1.14$ nm film ruptured at 4350 ps. This comparison shows that NaCl does not have a remarkable effect on film rupture. The TIP4P water model also was applied to study the effect of ions. The simulation run time for the $3 \times 3 \times 1.0$ nm TIP4P water film was 4 ns, and the water film was intact throughout the simulation. Eight Na^+ and Cl^- ions then were added to the water film, and again, the water film was intact after the 4 ns run time.

3.6. Analysis of the Relationship among $L_x = L_y/L_z$, CRT, and the Effect of Ions. CRT and critical thickness are two ways to describe the dynamic process of film rupture. CRT is concerned with the evolution of time, whereas critical thickness deals with the scale ratio $(L_x = L_y)/L_z$ when time is fixed. By increasing the value of the ratio $(L_x{=}L_y)/L_z$, the probability of rupture of the water film increases. Overall, NaCl did not appear to have a strong effect on the rupture of the nanofilm.

4. CONCLUSIONS

MD simulations of film rupture processes were performed to determine if general predictions of the CRT and critical thickness of water films could be achieved. CRT is an important parameter when applied to large-scale simulations, and its determination by simulation could be used to assist experimental efforts. The proposal of this new criterion can shed light on the correlation between the rupture process and thermodynamic properties. The combination of MD simulation of films and Gibbs dividing ranges is a new interpretation for film and interface related research. Overall, Na^+ and Cl^- ions have an effect on the stability of films, but the effect is significantly weaker when compared with surfactants. In the future, we could use large-scale MD simulations to investigate the process, which will take into account all environmental factors and should be able to reproduce this phenomenon better.

■ ACKNOWLEDGMENT

We gratefully acknowledge the University of Queensland and the Chinese Government for the UQ-CSC (China Scholarship Council) postgraduate scholarship for Tiefeng Peng and the School of Chemical Engineering at the University of Queensland for the intellectual condition and environment. We also thank Phong T. Nguyen and other members in Chemical Engineering Department for their helpful discussions. This research also is supported under the Australian Research Council's Discovery Projects funding scheme (grant DP0985079). Part of this work was funded by the Division of Chemical Sciences, Geosciences, and Biosciences, Office of Basic Energy Sciences (BES), of the

Table 5. States of Film with NaCl Ions after 3 ns of Run Time[a,b]

	$3 \times 3 \times 0.8$ nm	$3 \times 3 \times 1.0$ nm	$4 \times 4 \times 1.0$ nm	$4 \times 4 \times 1.15$ nm	$6 \times 6 \times 1.2$ nm	$6 \times 6 \times 1.3$ nm
NaCl	B (100 ps)	U	B (1300 ps)	U	B (800 ps)	U

[a] Concentration of NaCl in this study is as follows: the 3×3 nm films contained 8 NaCl ions (8 Na^+, 8 Cl^-), the 4×4 nm films 15 ions (15 Na^+, 15 Cl^-), the 6×6 nm film contained 30 ions (30 Na^+, 30 Cl^-), and the $6 \times 6 \times 1.3$ nm films 30 Na^+, 30 Cl^- in 1508 water. The concentration of ions is ~1 M. This concentration is well above the transition concentration, 0.1 M, of bubble coalescence inhibition. Indeed, our experiments (ref 7) show that the NaCl films are stable. [b] U: unbroken films. B: film broken at the time given in the brackets.

U.S. Department of Energy (DOE). Pacific Northwest National Laboratory (PNNL) is operated by Battelle for DOE.

REFERENCES

(1) Christine, H. L.; Karakashev, S. I.; Nguyen, P. T.; Nguyen, A. V.; Craig, V. S. J. *Langmuir* **2009**, *25*, 9931–9937.
(2) Karakashev, S. I.; Manev, E. D.; Nguyen, A. V. *Colloids Surf., A* **2008**, *319*, 34–42.
(3) Karakashev, S. I.; Manev, E. D.; Tsekov, R.; Nguyen, A. V. *J. Colloid Interface Sci.* **2008**, *318*, 358–364.
(4) Karakashev, S. I.; Nguyen, A. V. *Colloids Surf., A* **2007**, *293*, 229–240.
(5) Karakashev, S. I.; Nguyen, A. V. *Langmuir* **2009**, *25*, 3363–3368.
(6) Karakashev, S. I.; Nguyen, A. V.; Manev, E. D. *J. Colloid Interface Sci.* **2007**, *306*, 449–453.
(7) Karakashev, S. I.; Nguyen, P. T.; Roumen, T.; Hampton, M. A.; Nguyen, A. V. *Langmuir* **2008**, *24*, 11587–11591.
(8) Qu, X.; Wang, L.; Karakashev, Stoyan I.; Nguyen, A. V. *J. Colloid Interface Sci.* **2009**, *337*, 538–547.
(9) Taran, E.; Hampton, M. A.; Nguyen, A. V.; Attard, P. *Langmuir* **2009**, *25*, 2797–2803.
(10) Tsekov, R.; Ivanova, D. S.; Slavchov, R.; Radoev, B.; Manev, E. D.; Nguyen, A. V.; Karakashev, S. I. *Langmuir* **2010**, *26*, 4703–4708.
(11) Yang, W.; Wu, R.; Kong, B.; Zhang, X.; Yang, X. *J. Phys. Chem. B* **2009**, *113*, 8332.
(12) Yang, W.; Yang, X. *J. Phys. Chem. B* **2010**, *114*, 10066.
(13) Bresme, F.; Faraudo, J. *Langmuir* **2004**, *20*, 5127–5137.
(14) Jang, S. S.; Goddard, W. A. *J. Phys. Chem. B* **2006**, *110*, 7992.
(15) Hampton, M. A.; Nguyen, A. V. *Adv. Colloid Interface Sci.* **2010**, *154*, 30–55.
(16) Zimmerman, W. B.; Tesař, V.; Bandulasena, H. C. H. *Curr. Opin. Colloid Interface Sci.* **2011**, *16*, 350–356.
(17) Radoev, B.; Stoeckelhuber, K. W.; Tsekov, R.; Letocart, P. *Colloids Interface Sci. Ser.* **2007**, *3*, 151–172.
(18) Ajaev, V. S. *Phys. Fluids* **2006**, *18*, 068101/1–068101/4.
(19) Nguyen, A. V.; Schulze, H. J. *Colloidal Science of Flotation*; Marcel Dekker: New York, 2004; p 840.
(20) Benjamin, I. *Chem. Rev.* **2006**, *106*, 1212–1233.
(21) Chang, T. M.; Dang, L. X. *Chem. Rev.* **2006**, *106*, 1305–1322.
(22) Jungwirth, P.; Tobias, D. J. *Chem. Rev.* **2006**, *106*, 1259–1281.
(23) Hu, J. H.; Shi, Q.; Davidovits, P.; Worsnop, D. R.; Zahniser, M. S.; Kolb, C. E. *J. Phys. Chem.* **1995**, *99*, 8768–8776.
(24) Magi, L.; Schweitzer, F.; Pallares, C.; Cherif, S.; Mirabel, P.; George, C. *J. Phys. Chem. A* **1997**, *101*, 4943–4949.
(25) Thomas, J. L.; Jimenez-Aranda, A.; Finlayson-Pitts, B. J.; Dabdub, D. *J. Phys. Chem. A* **2006**, *110*, 1859–1867.
(26) Knipping, E. M.; Lakin, M. J.; Foster, K. L.; Jungwirth, P.; Tobias, D. J.; Gerber, R. B.; Dabdub, D.; Finlayson-Pitts, B. J. *Science* **2000**, *288*, 301.
(27) Petersen, P. B.; Saykally, R. J. *Chem. Phys. Lett.* **2004**, *397*, 51–55.
(28) Raymond, E. A.; Richmond, G. L. *J. Phys. Chem. B* **2004**, *108*, 5051–5059.
(29) Berendsen, H. J. C.; Spoel, D.v.d.; Drunmen, R. V. *Comput. Phys. Commun.* **1995**, *91*, 43–56.
(30) Hess, B.; Kutzner, C.; Spoel, D.; Lindahl, E. *J. Chem. Theory Comput.* **2008**, *4*, 435–447.
(31) Lindahl, E.; Hess, B.; Spoel, D. v. d. *J. Mol. Model.* **2001**, *7*, 306–317.
(32) Spoel, D.; Lindahl, E.; Hess, B.; Groenhof, G.; Mark, A. E.; Berendsen, H. J. C. *J. Comput. Chem.* **2005**, *26*, 1701–1718.
(33) Berenden, H. J. C.; Grigera, J. R.; Straatsma, T. P. *J. Phys. Chem.* **1987**, *91*, 6269–6271.
(34) Dang, L. X.; Chang, T. M. *J. Chem. Phys.* **1997**, *106*, 8149.
(35) Ussman, U.; Perela, L.; Berkowitz, M. L.; Lee, H; Pedersen, L. G. *J. Chem. Phys.* **1995**, *103*, 8577–8593.
(36) Ryckaert, J.-P.; Ciccotti, G.; Berendsen, H. J. C. *J. Comput. Phys.* **1977**, *23*, 327–341.